A Micro-Engineered Airway Lung-Chip Models Key Features of Viral-Induced Exacerbation of Asthma

Running title: Modeling human viral-induced asthma exacerbation on chip.

J. Nawroth[1§*], C. Lucchesi[1§], D. Cheng[1], A. Shukla[1], J. Ngyuen[1], T. Shroff[1], K. Karalis[1], H-H. Lee[2], S. Alves[2], G. A. Hamilton[1*], M. Salmon[1,3], and R. Villenave[1*].

[1]Emulate, Inc., Boston, MA; [2]Merck Research Laboratories, Boston, MA; [3]formerly Merck Research Laboratories, Boston, MA

[§] Authors contributed equally to this work.

[*] Corresponding Authors: Remi Villenave, PhD, Roche, Basel CH-4070, Switzerland (ph: +41 79 759 04 52; email: remi.villenave@roche.com); Geraldine Hamilton, PhD, Emulate, Inc., Boston, MA 02210, USA (email: geraldine.hamilton@emulatebio.com); Janna Nawroth, PhD, Hastings Center for Pulmonary Research, USC Keck School of Medicine, University of Southern California, Los Angeles, CA 90033, USA (email: jnawroth@usc.edu);

21 **At a Glance Commentary.**

22 **Scientific Knowledge on the Subject:** New therapies for asthma exacerbations remain
23 a significant unmet medical need. Development of human relevant preclinical models are
24 needed to further elucidate the complex mechanisms underlying asthma exacerbation
25 and investigate new therapeutic strategies.

26 **What This Study Adds to the Field:** Using a human Airway Lung-Chip model, we show
27 here for the first time a live human rhinovirus (HRV) infection of the asthmatic epithelium
28 that recapitulates complex features of viral-induced asthma exacerbation. The dynamic
29 microenvironment of the chip enables the real-time study of virus infection, epithelial
30 response, and immune cell recruitment under healthy and asthmatic conditions. The
31 model reproduces key endpoints that have been observed in asthmatics and individuals
32 infected with rhinovirus including the ciliated cell sloughing, altered cilia beating
33 frequency, goblet cell hyperplasia, increased expression of adhesion molecules in
34 microvascular endothelial cells, and inflammatory mediator release. High-resolution
35 temporal analysis of secreted inflammatory markers enabled by dynamic sampling
36 revealed alteration of IL-6, IFN-λ1 and CXCL10 secretory phases after rhinovirus infection
37 in an IL-13 high environment. Leveraging high-content imaging and analysis of circulating
38 inflammatory cells, we demonstrated the efficacy of a CXCR2 antagonist to reduce
39 adhesion, motility, and transmigration of perfused human neutrophils. Thus, this micro-
40 engineered chip may offer a powerful addition to preclinical models for understanding
41 mechanisms underlying asthma exacerbation pathology and developing new therapeutic
42 strategies.

Abstract

Rationale: Viral-induced exacerbation of asthma remain a major cause of hospitalization and mortality. New human relevant models of the airways are urgently needed to understand how respiratory infections may trigger asthma attacks, and to advance treatment development.

Objectives: To develop a new human relevant model of rhinovirus-induced asthma exacerbation that recapitulates viral infection of asthmatic airway epithelium, neutrophil transepithelial migration, and enables evaluation of immunomodulatory therapy.

Methods: A micro-engineered model of fully differentiated human mucociliary airway epithelium was stimulated with IL-13 to induce a Th2-type asthmatic phenotype and infected with live human rhinovirus 16 (HRV16) to reproduce key features of viral-induced asthma exacerbation.

Measurements and Main Results: Infection with HRV16 replicated key hallmarks of the cytopathology and inflammatory responses observed in human airways. Generation of a Th2 microenvironment through exogenous IL-13 stimulation induced features of asthmatics airways, including goblet cell hyperplasia, reduction of cilia beating frequency, and endothelial activation, but did not alter rhinovirus infectivity or replication. High resolution kinetic analysis of secreted inflammatory markers revealed that IL-13 treatment altered the IL-6, IFN-λ1, and CXCL10 secretion in response to HRV16. Neutrophil transepithelial migration was greatest when viral infection was combined with IL-13 treatment, while treatment with MK-7123, a CXCR2 antagonist, reduced neutrophil diapedesis in all conditions.

Conclusions: This micro-engineered Airway Lung-Chip provides a novel human-relevant platform for exploring the complex mechanisms underlying viral-induced asthma exacerbation. Our data suggest that IL-13 may impair the hosts' ability to mount an appropriate and coordinated immune response to rhinovirus infection. We also show that the Airway Lung-Chip can be used to assess the efficacy of modulators of the immune response.

Key words: asthma exacerbation, rhinovirus, Organ-on-chip, Airway Lung-Chip, immune response, high-content imaging

Note: Emulate®, Human Emulation System®, S-1™, ER-1™, and ER-2™ are trademarks of Emulate, Inc., and any other trademarks used herein remain with their respective holders. The technology disclosed in this document may be covered by one or more patents or patent applications, and no license to these is granted herein. You are solely responsible for determining whether you have all intellectual property rights that are necessary for your intended use of any of the disclosed materials, and whether you are required to obtain any additional intellectual property rights from a third party. Further information is available by contacting the authors.

Introduction.

Asthma is a chronic inflammatory disease of the respiratory tract defined by shortness of breath, wheezing, and chest tightness that affects 300 million people worldwide[1]. In most cases the disease can be managed with inhaled corticosteroids and bronchodilators; however, up to 1/8 of patients experience asthma exacerbations that can lead to emergency hospitalizations and death[2]. Asthma exacerbations are characterized by acute episodes of decreased lung function and result in significant morbidity, mortality and economic costs[3,4]. Prevention and treatment of asthma attacks hence remain an area of considerable unmet medical need[5]. A major trigger of asthma attacks is human rhinovirus (HRV) infection of asthmatic airways[6–8]. New human-relevant models are critically needed to study how a respiratory infection may provoke asthma attacks, and to advance the development of therapeutics[9]. To address this challenge, we leveraged a human Airway Lung-Chip featuring mucociliary airway epithelium and hemodynamic perfusion[10] to model key elements of viral-induced exacerbation of asthma. Our platform recapitulates (1) the asthmatic remodeling of human mucociliary airway epithelium, such as goblet cell hyperplasia[11], (2) cytopathic effects and epithelial inflammation in response to HRV infection[12], and (3) recruitment of immune cells to the epithelium[13]. We show that in conjunction with innovative high-content imaging, microfluidic sampling, and compound testing, the Airway Lung-Chip helps to elucidate and probe the pathological mechanisms that arise from the interaction of HRV infections with asthmatic airways, including impaired interferon responses and altered immune cell transmigration. Taken together, we demonstrate that our human Airway Lung-Chip provides a powerful new platform for

103 studying the time course, mechanisms and potential treatments of viral-induced asthma
104 exacerbations.

105

106 **Methods.**

107 Complete methods can be found in the online supplement.

108 **Cell differentiation and HRV infection on-chip.**

109 Cells were cultured and differentiated as previously described [10]. Briefly, human primary
110 airway epithelial cells (hAECs) from 4 healthy donors (Supplementary Table 1) were
111 seeded in the Airway Lung-Chips on a human placenta collagen IV-coated 3-µm pore
112 polyester membrane at a density of 3 x 10^6 cells/mL and left to attach for 2h. Five days
113 post seeding, air liquid interface (ALI) was introduced and Airway Lung-Chips were
114 perfused basally at 60µL/h for 3 weeks until full differentiation. Epithelium integrity,
115 ciliation, and apical mucus secretion were monitored for quality control. Upon full epithelial
116 differentation, hMVECs or HUVECs were seeded onto the opposite side of the
117 membrane, in the vascular channel at a density of 1 x 10^7 cells/mL and cultured under
118 flow for 3-4 days in endothelial growth media. Rhinovirus strain 16 (HRV-16) (ATCC® VR-
119 283) was inoculated into the epithelial channel of fully differentiated Airway Lung-Chips
120 and incubated for 3h at 33˚C while control chips received DMEM only. Following
121 incubation, the epithelial channel of each chip was gently rinsed 5 x with DMEM. After the
122 final wash, and every 24h thereafter, the epithelial surface was washed with 50 µL of
123 DMEM to determine virus growth kinetics and the basolateral effluent was collected for
124 cytokine/chemokine responses. HRV16 titers were determined by infecting H1-HeLa cells

125 (CRL-1958) with serially diluted virus samples, recording the number of wells positive for
126 viral cytopathic effect (CPE) at each dilution after 5 days post infection and calculating
127 the $TCID_{50}$/mL. A Th2 microenvironment was induced by perfusing the vascular channel
128 of the Airway Lung-Chips with 100 ng/mL of IL-13 (Peprotech, USA) for 7 days. High-
129 content imaging was performed in live and fixed tissues and followed by quantitative
130 analysis to extract structural and kinematic endpoints, including ciliary beat frequency and
131 neutrophil recruitment dynamics. Anti-dsRNA antibody J2 (mabJ2, scicons, CZR) was
132 utilized to detect replicating intracellular HRV16 by immunofluorescence staining.

133 **Results.**

134 Here, we describe the development of a human Airway Lung-Chip suitable for the study
135 of viral-induced asthma exacerbation and the effect of immunomodulatory compounds on
136 immune cell dynamics (**Supplementary Fig. 1A**).

137 **Adapting the Airway Lung-Chip design to enable immune cell transmigration.**

138 We adapted our recently developed micro-engineered "small-airway-on-a-chip" model [10]
139 by increasing the membrane pore size (3.0 µm vs 0.4 µm) to allow immune cells to
140 transmigrate from the vascular microchannel to the epithelial lumen (**Supplementary Fig.**
141 **1B**). As substrate pore size can greatly influence tissue differentiation[14], we validated the
142 new chip design for airway tissue culture. hAECs were seeded in the top channel and
143 human primary endothelial cells were seeded in the bottom channel to create a tissue-
144 tissue interface. We confirmed establishment of a well-differentiated mucociliary
145 bronchiolar epithelium by the presence of robust ZO-1-containing tight junctions,
146 characteristic epithelial cobblestone-like morphology, mucus producing goblet cells, and

147 dense coverage with ciliated cells (**Supplementary Fig. 1C-E)**. Formation of an intact
148 microvascular endothelium was validated by staining for endothelial junctional protein VE-
149 Cadherin (**Supplementary Fig. 1F)**. Mucociliary function was assessed by high-speed
150 video microscopy and quantitative analysis[15]. We measured a ciliary beat frequency of
151 16.35 (± 2.6) Hz (**Supplementary Fig. 1G-H, Supplementary movie 1**). Microbead
152 trajectories revealed locally unidirectional mucociliary transport (**Supplementary Fig. 1I**)
153 with a typical velocity of ~ 100 µm/sec, which is similar to mucociliary transport velocities
154 in intact human airways [16]. In sum, the Airway Lung-Chip was functionally augmented
155 with a 3-µm pore membrane to enable immune cell transmigration, and we validated that
156 it supports the viability and function of normal human bronchiolar tissue.

157

158 **HRV16 readily infects the Airway Lung-Chip and induces cytopathic effects.**

159 We next investigated HRV infection of the Airway Lung-Chip (**Fig. 1A)**. We infected the
160 chip apically with HRV16, a rhinovirus serotype commonly used in clinical challenge
161 studies, and analyzed viral infectivity and replication, cell tropism and induced cytopathic
162 effects (CPE). Infection a multiplicity of infection (MOI) of 1 resulted in a rapid apical
163 release of infectious virus particles that peaked between 24 and 48 hours post infection
164 (hpi) followed by a steady decline of released virions until no virus was detected 144 hpi
165 (**Fig. 1B**). This timeframe is consistent with viral shedding and symptom score profiles of
166 individuals experimentally infected with HRV [17–19].

167 HRV16 readily infected the intact epithelium and induced apical cell sloughing by 24 hpi
168 (**Fig. 1C**). Real time imaging and immunofluorescence (IF) characterization identified that

169 the majority of detached cells were infected multiciliated cells (**Fig. 1D, Supplementary**
170 **movie 2**), similar to what has been observed in respiratory tissue biopsies of human
171 volunteers experimentally infected with HRV[20,21]. Many of the detached cells were
172 TUNEL-positive, indicating apoptosis (**Supplementary Fig. 2A**). IF imaging of infected
173 chips revealed that HRV16 infection was restricted to ciliated cells and induced the
174 protrusion and extrusion of infected cells from the epithelial lining, while mucus producing
175 cells remained non-infected (**Fig.1E, Supplementary movie 2**). By day 6 post infection,
176 few ciliated cells remained on the epithelial surface (13-fold decrease in cilia coverage;
177 $p<0.001$) (**Fig. 1F, Supplementary Fig. 2B**) and they displayed significantly shorter cilia
178 (**Supplementary Fig 2C-D**). Additionally, consistent with HRV16 ciliated cell tropism, we
179 observed a 60% reduction in ciliary beat frequency following infection ($p<0.001$) (**Fig. 1G**
180 and **Supplementary movie 3**). The acute damage to ciliated cells was accompanied by
181 a 2-fold increase in the area covered by MUC5AC positive cells by day 6 post infection
182 compared to non-infected chips ($p<0.001$) (**Fig. 1H, Supplementary Fig. 2E**), in line with
183 clinical observations[22].

184

185 **Modeling viral-induced asthma exacerbation on-chip.**

186 We used interleukin-13 (IL-13) stimulation to induce features of type 2 inflammation in
187 asthma (**Fig. 1I**). IL-13 plays a central role in allergic asthma and, together with IL-5, is
188 an important mediator of viral-induced exacerbations in asthma [23]. When we perfused the
189 vascular channel of the Airway Lung-Chip with IL-13 (100 ng/mL) for 7 days preceding
190 virus infection we detected a significant increase in the number of goblet cells (rising from
191 16.5% to 50.3% total area; $p<0.01$) (**Fig. 1K, Supplementary Fig. 3**) and a decrease in

192 cilia beating frequency (14.4% reduction; $p<0.001$) (**Fig. 1K,L and Supplementary**
193 **movie 4**), which is consistent with observations made in airway mucosa of asthmatic
194 patients [24,25].

195 To recapitulate HRV-induced asthma exacerbation, we combined IL-13 treatment with
196 HRV16 infection to induce exacerbation (**Fig. 2A**). Infection of the IL-13 stimulated Airway
197 Lung-Chip with HRV16 did not result in significant changes in viral loads in apical washes
198 nor in the duration of infection when compared with non-stimulated chips (**Fig. 2B**). This
199 finding is consistent with recent studies in asthmatics experimentally infected with HRV16
200 [26–28], although another study found a higher viral load in asthmatics on day 3 of infection[29].

201 Type 2 inflammation has been suggested to increase asthmatics susceptibility to
202 exacerbations through airway remodeling and modulation of the antiviral response [30]. To
203 gain insight into the effect of IL-13 on HRV16-induced inflammatory responses we first
204 measured the levels of pro-inflammatory cytokines and chemokines released apically and
205 basolaterally at 24, 48 and 72 h post HRV16 infection, in the presence or absence of IL-
206 13 (**Fig.2C-E and Supplementary Fig. 4**). Apical and basolateral secretion of CCL11
207 (Eotaxin-1), a potent eosinophil chemoattractant and marker of Th2 asthma in human [31],
208 was increased following HRV16 infection (**Fig. 2C**), consistent with literature[32]. This was
209 not significantly altered by IL-13 treatment. In contrast and consistent with literature[33],
210 apical secretion of CCL26 (Eotaxin-3), another chemokine associated with eosinophil
211 recruitment and persistence in patients with asthma[34], was increased at all time points
212 following stimulation with IL-13 alone, while HRV16 infection had no effect on CCL26
213 release. Analysis of the interferon (IFN) type III responses revealed that apical and basal
214 release of IFN-λ1 at 48 hpi, and of the IFN-induced lymphocyte chemoattractant CXCL10

215 at 48 and 72 hpi were increased following HRV16 infection (**Fig. 2D**). IL-13 treatment
216 significantly reduced the measured IFN response in HRV16 infected chips. This is
217 consistent with other in vitro studies showing that IL-13 impairs IFN-λ production[35], and
218 with clinical reports intimating that individuals with asthma or cells from asthmatics
219 infected with HRV have a deficient IFN response [36–39], although this remains
220 controversial[40]. Basal secretion of IL-8, a potent attractant of neutrophils[41], was increased
221 48 h post HRV16 infection, with little impact of IL-13 treatment (**Fig. 2E**). In contrast, we
222 found that induction of IL-6 secretion following HRV16 infection was greatly reduced in
223 IL-13 treated samples at 48 h post infection (**Fig. 2E)**. Notably, we did not detect any IFN-
224 β secretion at any time point with and without IL-13 stimulation.

225 To elucidate the kinetics of inflammatory mediator release during viral-induced asthma
226 exacerbations and thereby gain additional insight into the pathophysiological process[42,43],
227 we exploited the microperfusion of the Airway Lung-Chip for high resolution temporal
228 profiling of IFN-λ1, CXCL10 and IL-6 secretion. By collecting basal medium outflow every
229 2h for 74h, we revealed the temporal dynamics of cytokine secretion after HRV infection
230 (**Fig. 2F**). In untreated chips, both IFN-λ1 and IL-6 increased quickly and reached
231 maximal, or near maximal, values at approximately 22 h post HRV16 infection. CXCL10
232 rose more slowly and peaked at 34 h post infection, in line with direct interferon-
233 dependent regulation of CXCL10. In contrast, the IL-13 treated chips exhibited markedly
234 suppressed secretion profiles. The high-resolution profiling plots reveal this difference in
235 the first 24h, whereas it remains masked in the accumulated medium collected after 24
236 hpi (**Fig. 2D,E**). This demonstrates that high resolution profiling is a sensitive method for

237 detecting onset and dynamics of cytokines release, determining sensitive time windows,
238 and identifying the best sampling strategy.

239 We also investigated the effect of the IL-13 stimulation of human endothelial cells, which
240 contributes to leukocyte recruitment in the pathogenesis of asthma[44]. Within 48h of the
241 IL-13 treatment, we observed progressive endothelium morphological changes leading to
242 the formation of cell aggregates throughout the vascular wall (**Supplementary Fig. 5A**)
243 accompanied by a doubling of endothelial cell density ($p < 0.0001$) (**Supplementary Fig.**
244 **5B**). Further analysis revealed increased gene expression of P-Selectin ($p = 0.036$) and
245 E-Selectin ($p = 0.06$), two adhesion molecules involved in inflammatory cell recruitment,
246 compared to control (**Supplementary Fig. 5C, Supplementary Table 2**). IF staining of
247 intercellular adhesion molecule 1 (ICAM-1) and vascular cell adhesion protein 1 (VCAM-
248 1) was also increased in IL-13 treated cultures (**Supplementary Fig. 5E)**, indicating that
249 IL-13 promotes activation of the lung microvascular endothelium. Indeed, bronchial
250 biopsies from subjects with asthma revealed increased adhesion molecule expression in
251 endothelial cells[45].Although we cannot rule out that the IL-13 treatment stimulated the
252 epithelial cells to release additional chemokines, our findings align with previous studies
253 on the effects of IL-13 on human endothelial cells[46].

254

255 **Pharmacological modulation of neutrophil recruitment and transmigration by a**
256 **CXCR2 antagonist on-chip.**

257 Airway neutrophilia is frequently observed in acute exacerbations of asthma[13,47,48], and is
258 associated with asthma severity[49]. HRV infections in asthmatics may also promote

259 selective recruitment of neutrophils[50]. Since neutrophils can contribute to asthma
260 exacerbation through the release of tissue-damaging compounds[51], neutrophil
261 recruitment constitutes a potential drug target. We sought to show feasibility of probing
262 the real-time dynamics of neutrophil recruitment on the Airway Lung-Chip, where the
263 endothelial vascular channel supports the live observation of circulating and
264 transmigrating neutrophils. In a proof-of-concept study, we investigated neutrophil
265 recruitment in exacerbated conditions and in response to a CXCR2 antagonist, which
266 blocks neutrophil sensing of IL-8[41]. Here, we perfused freshly isolated human neutrophils
267 stained with a live dye through the vascular channel of exacerbated asthma chips under
268 physiological flow (i.e., with fluid shear stresses of ca. 1 dyn/cm^2 [52], an important factor
269 for physiological neutrophil recruitment[53]). We observed neutrophil adhesion and crawling
270 at the surface of the microvascular endothelium, rapidly followed by neutrophil
271 transendothelial migration through a combination of transcellular and paracellular
272 migratory events (**Fig. 3A, B**). Treatment with either IL-13 or HRV16 significantly
273 increased neutrophil adhesion, and combined treatment almost doubled recruitment
274 compared to each condition alone (**Fig. 3C, D**). Pre-treatment of neutrophils with 10 μM
275 MK-7123, a CXCR2 antagonist, at 24 hpi significantly reduced neutrophil adhesion to the
276 endothelium in all treatment groups (**Fig. 3C, D**), and also reduced neutrophil crawling
277 velocity (**Fig. 3E, F and Supplementary movies 5 and 6**). Real time imaging revealed
278 that many endothelium bound neutrophils transmigrated from the vascular channel
279 through the 3-μm pores of the membrane (which frequently merge into even larger pores
280 in track-etched membranes) into the epithelium channel where they adhered to the
281 epithelial surface (**Fig. 3G and Supplementary movie 7**) and treatment with MK-7123

282 reduced the proportion of transmigrating neutrophils (**Fig. 3H**). Furthermore,
283 characterization of fully migrated neutrophils revealed expression of myeloperoxidase
284 (**Fig. 3I**), a marker of neutrophil activation found in lungs of asthmatics [54] that contributes
285 to inflammation *in vivo* [55]. Thus, our on-chip disease model of asthma exacerbation not
286 only enabled efficacy testing of an immunomodulatory compound but also elucidated the
287 multi-step dynamics of neutrophil recruitment in a human-relevant context.

288

289 **Discussion**

290 We still incompletely understand why asthmatics are at higher risk of developing life-
291 threatening exacerbation following rhinovirus infection. Previous *in vitro* studies have
292 suggested that prior damage to the asthmatic airway epithelium facilitates HRV infection
293 by exposing more permissive, ICAM-1-expressing basal cells, explaining the
294 susceptibility of asthmatic airways to infection [56,57]. The corollary is the perception that
295 intact epithelial layers of healthy subjects are somewhat resistant to HRV infection[58].
296 Contrasting with this view, our findings demonstrate that HRV can readily infect the intact
297 well-differentiated mucociliary epithelium and induce significant airway remodeling
298 leading to almost complete loss of ciliated cells and goblet cell hyperplasia by day 7 post
299 infection. Our observations are consistent with studies showing induction of mucin
300 production by rhinovirus infection of human bronchial epithelia in vitro and in vivo [22,59],
301 the induction of goblet cell metaplasia by rhinovirus-mediated foxa3 activation[60], high viral
302 load and cell shedding the airways of individuals infected with HRV[20,26–28], as well as
303 HRV-induced CPEs[61,62] and apoptotic events[63] in *in vitro* human bronchial epithelia. This
304 suggests that RV infections have considerable potential for cytopathic and remodeling

305 effects in the airways, and that HRV-induced CPE might contribute to exacerbations in
306 asthmatic individuals by directly damaging mucociliary clearance and increasing mucus
307 secretion.

308 Several groups have investigated the effect of IL-13-induced mucous metaplasia on the
309 susceptibility of human airway epithelium to HRV infection and come to discordant
310 conclusions, such as increased versus reduced susceptibility to HRV infection [64 65]. In
311 contrast, we did not detect any significant difference in viral load or infection persistence
312 in IL-13 treated versus non-treated chips. Donor to donor variability and differences in
313 experimental design might explain the different outcomes. Clinical studies are also in
314 disagreement, with some reporting higher viral loads in asthmatics[29] while others align
315 with our results in showing no difference in viral titer of asthmatics compared to non-
316 asthmatics [26–28,66]. In sum, there are clearly many remaining unknowns in HRV-induced
317 asthma exacerbation, and our findings show that the Airway Lung-Chip is a valuable new
318 tool for their investigation.

319 We found that HRV-induced type III IFN response was ablated in a type 2
320 microenvironment, which is consistent with studies showing impaired IFN responses in
321 cells from asthmatic individuals challenged with HRV [36,67]. However, several recent *in*
322 *vitro* and *in vivo* studies contradict these results [26,28,40,68,69], suggesting that an impaired
323 IFN responses may not be the only factor contributing to exacerbation. Asthma phenotype
324 heterogeneity and differences in the study designs may further confound the picture. An
325 impaired IFN response might be specific to asthmatics with a Th2-dominant inflammatory
326 profile [23,36], in line with the downregulation of IFN-λ1 by a Th2 microenvironment on our
327 chip.

328 Effective orchestration and resolution of the immune response rely on both magnitude
329 and kinetics of secreted cytokines. IL-6 is a prime example as its pro- or anti-inflammatory
330 nature depends on secretion timing [43]. Here, we have leveraged the microscale perfusion
331 of the Airway Lung-Chip to conduct high resolution temporal profiling of secreted
332 cytokines. We found that the IL-6 secretory profile was markedly disrupted by IL-13
333 stimulation. This could be due to the altered epithelial architecture and cell type
334 composition of the asthmatic microenvironment[70], which may alter cytokine
335 responses[71,72]. The central role of IL-6 in infection and inflammation has been extensively
336 described [73] and though it is usually considered a pro-inflammatory mediator in asthma
337 exacerbations, its protective role in the lung was highlighted in several studies [42 74 75 76],
338 which together with our results may suggest a more nuanced role for IL-6 in exacerbation
339 pathogenesis.

340 We also demonstrated the utility of the Airway Lung-Chip for testing the efficacy of
341 immunomodulatory compounds on neutrophil recruitment. Though the first generation of
342 CXCR2 inhibitors has failed to deliver in the clinic, it is now appreciated that neutrophils
343 are extremely heterogeneous and display different responses depending on subtype and
344 environmental factors[77]. Because of this, more than ever new platforms like the Airway
345 Lung-Chip are needed to enable the phenotypic and functional profiling of neutrophils in
346 the context of disease and drug treatment.

347 In summary, we developed a new on-chip human disease model of viral-induced asthma
348 exacerbations that recapitulates hallmarks of rhinovirus-induced responses of the
349 asthmatic airway. Owing to its unique fluidic design and accessibility to optical imaging,
350 the Airway Lung-Chip also enables the high-resolution profiling of cytokine release,

351 phenotypic changes and dynamic immune cell responses to immunomodulatory
352 therapies in a human-relevant context, thus adding a powerful pre-clinical platform for
353 probing complex disease mechanisms and developing new treatments for asthma
354 exacerbations.

355

356 **Acknowledgments.**

357 We thank Dr. Anne van der Does and Dr. Gurpreet Brar for the critical review of the
358 manuscript and Brett Clair for his assistance with graphic design.

359

360 **Declaration of Interests.**

361 C.L., J.N., A.S., J.N., K.K., T.S, G. H, and R.V. are current or former employees and hold
362 equity of Emulate, Inc.

363

364 **References.**

365 1. Masoli, M., Fabian, D., Holt, S., Beasley, R. & Global Initiative for Asthma (GINA)
366 Program. The global burden of asthma: executive summary of the GINA
367 Dissemination Committee report. *Allergy* **59**, 469–78 (2004).

368 2. Suruki, R. Y., Daugherty, J. B., Boudiaf, N. & Albers, F. C. The frequency of
369 asthma exacerbations and healthcare utilization in patients with asthma from the
370 UK and USA. *BMC Pulm. Med.* **17**, 74 (2017).

3. Watson, L., Turk, F., James, P. & Holgate, S. T. Factors associated with mortality after an asthma admission: A national United Kingdom database analysis. *Respir. Med.* **101**, 1659–1664 (2007).

4. Smith, K. *et al.* Evaluation of Risk Factors and Health Outcomes among Persons with Asthma. *J. Asthma* **46**, 234–237 (2009).

5. Castillo, J. R., Peters, S. P. & Busse, W. W. Asthma Exacerbations: Pathogenesis, Prevention, and Treatment. *J. allergy Clin. Immunol. Pract.* **5**, 918–927 (2016).

6. Holgate, S. T. Rhinoviruses in the pathogenesis of asthma: The bronchial epithelium as a major disease target. *Journal of Allergy and Clinical Immunology* vol. 118 587–590 (2006).

7. Jackson, D. J. & Johnston, S. L. The role of viruses in acute exacerbations of asthma. *J. Allergy Clin. Immunol.* **125**, 1178–87; quiz 1188–9 (2010).

8. Johnston, S. L. *et al.* Community study of role of viral infections in exacerbations of asthma in 9-11 year old children. *BMJ* **310**, 1225–1229 (1995).

9. Holmes, A. M., Solari, R. & Holgate, S. T. Animal models of asthma: value, limitations and opportunities for alternative approaches. *Drug Discov. Today* **16**, 659–70 (2011).

10. Benam, K. H. *et al.* Small airway-on-a-chip enables analysis of human lung inflammation and drug responses in vitro. *Nat. Methods* **13**, 151–7 (2016).

11. Davies, D. E. The role of the epithelium in airway remodeling in asthma.

Proceedings of the American Thoracic Society vol. 6 678–682 (2009).

12. Papadopoulos, N. G. *et al.* Rhinoviruses Infect the Lower Airways. *J. Infect. Dis.* **181**, 1875–1884 (2000).

13. Fahy, J. V. Eosinophilic and neutrophilic inflammation in asthma: insights from clinical studies. *Proc. Am. Thorac. Soc.* **6**, 256–9 (2009).

14. Bružauskaitė, I., Bironaitė, D., Bagdonas, E. & Bernotienė, E. Scaffolds and cells for tissue regeneration: different scaffold pore sizes—different cell effects. *Cytotechnology* vol. 68 355–369 (2016).

15. Benam, K. H. *et al.* Matched-Comparative Modeling of Normal and Diseased Human Airway Responses Using a Microengineered Breathing Lung Chip. *Cell Syst.* **3**, 456-466.e4 (2016).

16. Hofmann, W. & Asgharian, B. Comparison of Mucociliary Clearance Velocities in Human and Rat Lungs for Extrapolation Modeling. **46**, 323–325 (2002).

17. Hayden, F. G. *et al.* Intranasal pirodavir (R77,975) treatment of rhinovirus colds. *Antimicrob. Agents Chemother.* **39**, 290–294 (1995).

18. Gern, J. E. *et al.* Inhibition of rhinovirus replication in vitro and in vivo by acid-buffered saline. *J. Infect. Dis.* **195**, 1137–1143 (2007).

19. Igarashi, Y. *et al.* Analysis of nasal secretions during experimental rhinovirus upper respiratory infections. *J. Allergy Clin. Immunol.* **92**, 722–731 (1993).

20. Tumer, R. B., Hendley, J. O. & Gwaltney, J. M. Shedding of infected ciliated epithelial cells in rhinovirus colds. *J. Infect. Dis.* **145**, 849–853 (1982).

21. Mosser, A. G. *et al.* Quantitative and qualitative analysis of rhinovirus infection in bronchial tissues. *Am. J. Respir. Crit. Care Med.* **171**, 645–651 (2005).

22. Hewson, C. A. *et al.* Rhinovirus induces MUC5AC in a human infection model and in vitro via NF-κB and EGFR pathways. *Eur. Respir. J.* **36**, 1425–1435 (2010).

23. Fahy, J. V. Type 2 inflammation in asthma--present in most, absent in many. *Nat. Rev. Immunol.* **15**, 57–65 (2015).

24. Thomas, B. *et al.* Ciliary dysfunction and ultrastructural abnormalities are features of severe asthma. *J. Allergy Clin. Immunol.* **126**, 722-729.e2 (2010).

25. Ordoñez, C. L. *et al.* Mild and moderate asthma is associated with airway goblet cell hyperplasia and abnormalities in mucin gene expression. *Am. J. Respir. Crit. Care Med.* **163**, 517–23 (2001).

26. Kennedy, J. L. *et al.* Comparison of viral load in individuals with and without asthma during infections with rhinovirus. *Am. J. Respir. Crit. Care Med.* **189**, 532–539 (2014).

27. Denlinger, L. C. *et al.* Lower airway rhinovirus burden and the seasonal risk of asthma exacerbation. *Am. J. Respir. Crit. Care Med.* **184**, 1007–14 (2011).

28. DeMore, J. P. *et al.* Similar colds in subjects with allergic asthma and nonatopic subjects after inoculation with rhinovirus-16. *J. Allergy Clin. Immunol.* **124**, 245–52, 252.e1–3 (2009).

29. Jackson, D. J. *et al.* IL-33-Dependent type 2 inflammation during rhinovirus-induced asthma exacerbations in vivo. *Am. J. Respir. Crit. Care Med.* **190**, 1373–

1382 (2014).

30. Dunican, E. M. & Fahy, J. V. The Role of Type 2 Inflammation in the Pathogenesis of Asthma Exacerbations. *Ann. Am. Thorac. Soc.* **12 Suppl 2**, S144-9 (2015).

31. Wu, D. *et al.* CCL11 as a potential diagnostic marker for asthma? *J. Asthma* **51**, 847–854 (2014).

32. Papadopoulos, N. G. *et al.* Rhinovirus infection up-regulates eotaxin and eotaxin-2 expression in bronchial epithelial cells. *Clin. Exp. Allergy* **31**, 1060–1066 (2001).

33. Roberts, N., Al Mubarak, R., Francisco, D., Kraft, M. & Chu, H. W. Comparison of paired human nasal and bronchial airway epithelial cell responses to rhinovirus infection and IL-13 treatment. *Clin. Transl. Med.* **7**, (2018).

34. Ravensberg, A. J. *et al.* Eotaxin-2 and eotaxin-3 expression is associated with persistent eosinophilic bronchial inflammation in patients with asthma after allergen challenge. *J. Allergy Clin. Immunol.* **115**, 779–785 (2005).

35. Moriwaki, A. *et al.* IL-13 suppresses double-stranded RNA-induced IFN-λ production in lung cells. *Biochem. Biophys. Res. Commun.* **404**, 922–927 (2011).

36. Baraldo, S. *et al.* Deficient antiviral immune responses in childhood: distinct roles of atopy and asthma. *J. Allergy Clin. Immunol.* **130**, 1307–14 (2012).

37. Contoli, M., Message, S. & Laza-Stanca, V. Role of deficient type III interferon-λ production in asthma exacerbations. Supplements. *Nat. Med.* **1**, (2006).

38. Papadopoulos, N. G., Stanciu, L. A., Papi, A., Holgate, S. T. & Johnston, S. L. A

defective type 1 response to rhinovirus in atopic asthma. *Thorax* **57**, 328–332 (2002).

39. Wark, P. A. B. *et al.* Asthmatic bronchial epithelial cells have a deficient innate immune response to infection with rhinovirus. *J. Exp. Med.* **201**, 937–47 (2005).

40. Lopez-Souza, N. *et al.* In vitro susceptibility to rhinovirus infection is greater for bronchial than for nasal airway epithelial cells in human subjects. *J. Allergy Clin. Immunol.* **123**, 1384–90.e2 (2009).

41. Russo, R. C., Garcia, C. C., Teixeira, M. M. & Amaral, F. A. The CXCL8/IL-8 chemokine family and its receptors in inflammatory diseases. *Expert Rev. Clin. Immunol.* **10**, 593–619 (2014).

42. Jones, S. A. Directing transition from innate to acquired immunity: defining a role for IL-6. *J. Immunol. (Baltimore, Md. 1950)* **175**, 3463–3468 (2005).

43. Pyle, C. J., Uwadiae, F. I., Swieboda, D. P. & Harker, J. A. Early IL-6 signalling promotes IL-27 dependent maturation of regulatory T cells in the lungs and resolution of viral immunopathology. *PLoS Pathog.* **13**, 1–27 (2017).

44. Doran, E. *et al.* Interleukin-13 in asthma and other eosinophilic disorders. *Front. Med.* **4**, 139 (2017).

45. Ohkawara, Y. *et al.* In situ expression of the cell adhesion molecules in bronchial tissues from asthmatics with air flow limitation: in vivo evidence of VCAM-1/VLA-4 interaction in selective eosinophil infiltration. *Am. J. Respir. Cell Mol. Biol.* **12**, 4–12 (1995).

46. Kotowicz, K., Callard, R. E., Friedrich, K., Matthews, D. J. & Klein, N. Biological activity of IL-4 and IL-13 on human endothelial cells: functional evidence that both cytokines act through the same receptor. *Int Immunol* **8**, 1915–1925 (1996).

47. Fahya, b, J. V., Kimb, K. W., Liub, J. & Bousheya, b, H. A. Prominent neutrophilic inflammation in sputum from subjects with asthma exacerbation. *J. Allergy Clin. Immunol.* **95**, 843–852 (1995).

48. Ordoñez, C. L., Shaughnessy, T. E., Matthay, M. A. & Fahy, J. V. Increased neutrophil numbers and IL-8 levels in airway secretions in acute severe asthma: Clinical and biologic significance. *Am. J. Respir. Crit. Care Med.* **161**, 1185–1190 (2000).

49. Ray, A. & Kolls, J. K. Neutrophilic Inflammation in Asthma and Association with Disease Severity. *Trends in Immunology* vol. 38 942–954 (2017).

50. Jarjour, N. N. *et al.* The effect of an experimental rhinovirus 16 infection on bronchial lavage neutrophils. *J. Allergy Clin. Immunol.* **105**, 1169–1177 (2000).

51. Busse, W. W. A role for neutrophils in asthma exacerbations. *Nature Medicine* vol. 23 658–659 (2017).

52. Cheng, C. *et al.* Large variations in absolute wall shear stress levels within one species and between species. *Atherosclerosis* vol. 195 225–235 (2007).

53. Smith, L. A., Aranda-Espinoza, H., Haun, J. B. & Hammer, D. A. Interplay between shear stress and adhesion on neutrophil locomotion. *Biophys. J.* **92**, 632–640 (2007).

54. JATAKANON, A. *et al.* Neutrophilic Inflammation in Severe Persistent Asthma. *Am. J. Respir. Crit. Care Med.* **160**, 1532–1539 (1999).

55. Kolaczkowska, E. & Kubes, P. Neutrophil recruitment and function in health and inflammation. *Nat. Rev. Immunol.* **13**, 159–75 (2013).

56. Sajjan, U., Wang, Q., Zhao, Y., Gruenert, D. C. & Hershenson, M. B. Rhinovirus disrupts the barrier function of polarized airway epithelial cells. *Am. J. Respir. Crit. Care Med.* **178**, 1271–1281 (2008).

57. Lopez-Souza, N. *et al.* Resistance of differentiated human airway epithelium to infection by rhinovirus. *Am. J. Physiol. Lung Cell. Mol. Physiol.* **286**, L373–L381 (2004).

58. Gern, J. E. The ABCs of rhinoviruses, wheezing, and asthma. *J. Virol.* **84**, 7418–26 (2010).

59. Inoue, D. *et al.* Mechanisms of mucin production by rhinovirus infection in cultured human airway epithelial cells. *Respir. Physiol. Neurobiol.* **154**, 484–499 (2006).

60. Chen, G. *et al.* Foxa3 induces goblet cell metaplasia and inhibits innate antiviral immunity. *Am. J. Respir. Crit. Care Med.* **189**, 301–313 (2014).

61. Bossios, A. *et al.* Rhinovirus infection induces cytotoxicity and delays wound healing in bronchial epithelial cells. *Respir. Res.* **6**, 114 (2005).

62. Schroth, M. K. *et al.* Rhinovirus replication causes RANTES production in primary bronchial epithelial cells. *Am. J. Respir. Cell Mol. Biol.* **20**, 1220–1228 (1999).

63. Deszcz, L., Gaudernak, E., Kuechler, E. & Seipelt, J. Apoptotic events induced by

human rhinovirus infection. *J. Gen. Virol.* **86**, 1379–1389 (2005).

64. Lachowicz-Scroggins, M. E., Boushey, H. A., Finkbeiner, W. E. & Widdicombe, J. H. Interleukin-13-induced mucous metaplasia increases susceptibility of human airway epithelium to rhinovirus infection. *Am. J. Respir. Cell Mol. Biol.* **43**, 652–61 (2010).

65. Jakiela, B. *et al.* Th2-type cytokine-induced mucus metaplasia decreases susceptibility of human bronchial epithelium to rhinovirus infection. *Am. J. Respir. Cell Mol. Biol.* **51**, 229–241 (2014).

66. Fleming, H. E. *et al.* Rhinovirus-16 colds in healthy and in asthmatic subjects: Similar changes in upper and lower airways. *Am. J. Respir. Crit. Care Med.* **160**, 100–108 (1999).

67. Contoli, M. *et al.* Role of deficient type III interferon-lambda production in asthma exacerbations. *Nat. Med.* **12**, 1023–6 (2006).

68. Bochkov, Y. A., Hanson, K. M., Keles, S., Brockman-schneider, R. A. & Jarjour, N. N. Rhinovirus-induced modulation of gene expression in bronchial epithelial cells from subjects with asthma. *Mucosal Immunol.* **3**, 69–80 (2010).

69. Hansel, T. T. *et al.* EBioMedicine A Comprehensive Evaluation of Nasal and Bronchial Cytokines and Chemokines Following Experimental Rhinovirus Infection in Allergic Asthma : Increased Interferons (IFN- γ and IFN- λ) and Type 2 In fl ammation (IL-5 and IL-13). *EBioMedicine* **19**, 128–138 (2017).

70. Seibold, M. A. Interleukin-13 Stimulation Reveals the Cellular and Functional

Plasticity of the Airway Epithelium. **15**, (2018).

71. Tanabe, T. & Rubin, B. K. Airway goblet cells secrete pro-inflammatory cytokines, chemokines, and growth factors. *Chest* **149**, 714–720 (2016).

72. Xie, B. *et al.* Chemokine expression in the early response to injury in human airway epithelial cells. 1–22 (2018).

73. Hunter, C. A. & Jones, S. A. IL-6 as a keystone cytokine in health and disease. *Nat. Immunol.* **16**, 448–57 (2015).

74. Stumhofer, J. S. *et al.* Interleukins 27 and 6 induce STAT3-mediated T cell production of interleukin 10. *Nat. Immunol.* **8**, 1363–1371 (2007).

75. DiCosmo, B. F. *et al.* Airway epithelial cell expression of interleukin-6 in transgenic mice. Uncoupling of airway inflammation and bronchial hyperreactivity. *J. Clin. Invest.* **94**, 2028–35 (1994).

76. Beale, J. *et al.* Rhinovirus-induced IL-25 in asthma exacerbation drives type 2 immunity and allergic pulmonary inflammation. *Sci. Transl. Med.* **6**, 256ra134 (2014).

77. Silvestre-Roig, C., Fridlender, Z. G., Glogauer, M. & Scapini, P. Neutrophil Diversity in Health and Disease. *Trends in Immunology* vol. 40 565–583 (2019).

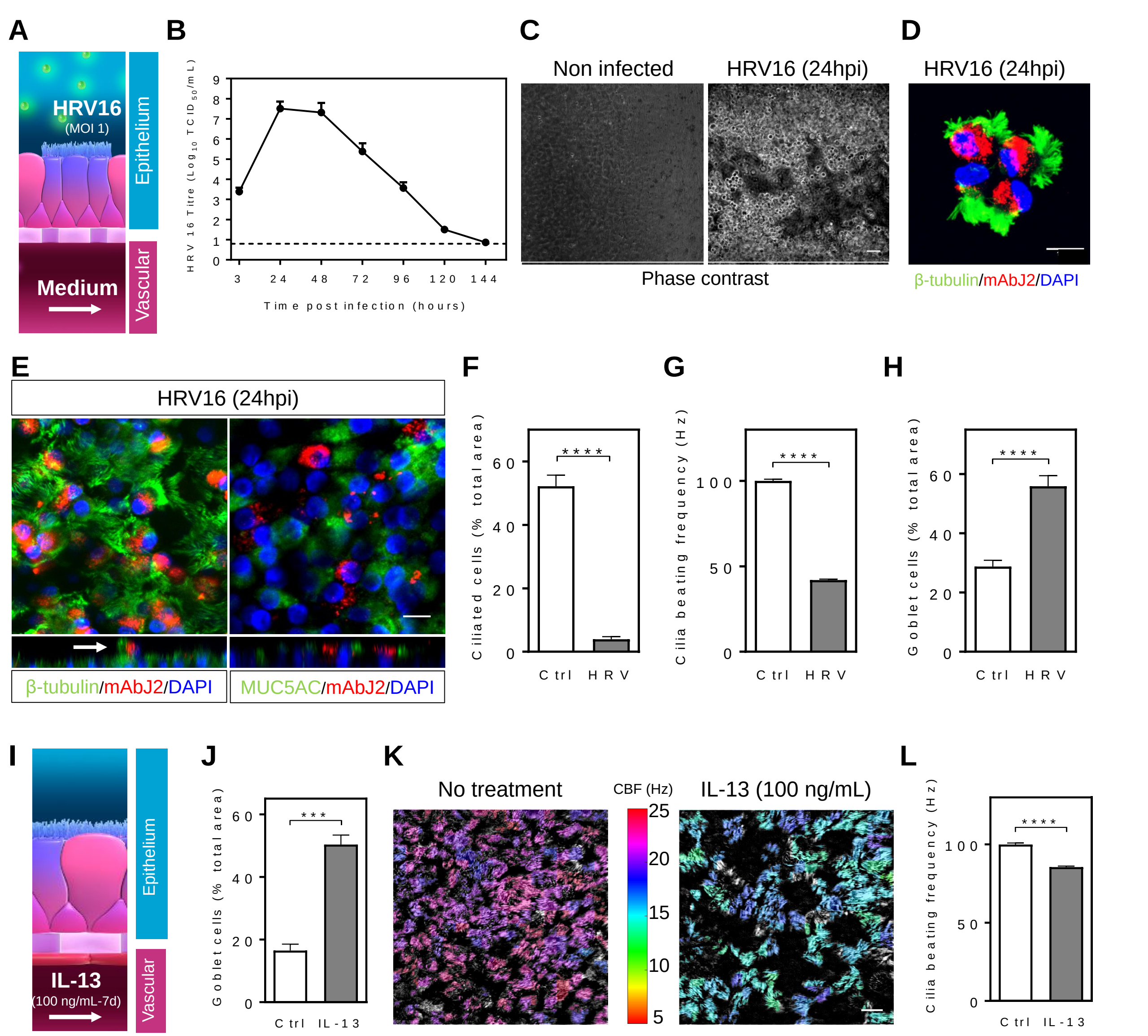

Fig 1. **Modeling HRV infection and Th2 asthma phenotype on the Airway Lung-Chip**. (**A**) HRV-16 was apically delivered to the chip at an MOI~1. (**B**) Viral growth kinetic of HRV-16 following infection. HRV16 was titrated in apical washes and data represent mean ± SD log10 $TCID_{50}$/ml from 3 different donors with two to five biological replicates per donor. The dashed line indicate the limit of detection of the titration assay. (**C**) Phase contrast micrographs of differentiated airway epithelium cultured in the airway chip for 3 weeks at air liquid interface infected with HRV16 for 24h (right) or non infected (left) showing epithelial cells sloughed off infected cultures while non infected epithelium remains intact. Scale bar, 50 µm. (**D**) IF image of apical washes from cultures infected with HRV16 for 24h showing detached cells stained for β-tubulin (green), mAbJ2 (red) and DAPI (blue). Scale bar, 10 µm. (**E**) IF image of the differentiated mucociliary epithelium on-chip infected with HRV16 for 24h and stained for β-tubulin (left) or MUC5AC (right) (green) and mAbJ2 (red). Orthogonal views show a ciliated infected cells protruding from the epithelial lining (white arrow). Scale bar, 20 µm. (**F**) Total culture area covered by ciliated cells in non infected chips and 6 days post HRV16 infection. (**G**) Cilia beating frequency in non infected chips and 72 hpi. (**H**) Total culture area covered by goblet cells in non infected control and HRV16 infected chips 6 dpi. (**I**) A Th2 asthma environment was generated through vascular perfusion of IL-13 (100 ng/mL) over 7 days. (**J**) Total culture area covered by goblet cells in absence or presence of IL-13 (100 ng/mL) for 7 days. (**K**) Heat map of cilia beating frequency (CBF) on-chip generated from a high speed recording of cilia beating in a representative field of view in absence or presence of IL-13 (100 ng/mL). Scale shows color coded CBF values in Hz. Scale bar, 20 µm. (**L**) Graph showing ciliary beat frequency in absence or presence of IL-13 (100 ng/mL). Data are from chips with cells from three healthy donors, with one or two biological replicates (chips) per donor. Data represent mean ±SEM and significance was determined by unpaired Student's; ****P < 0.0001.

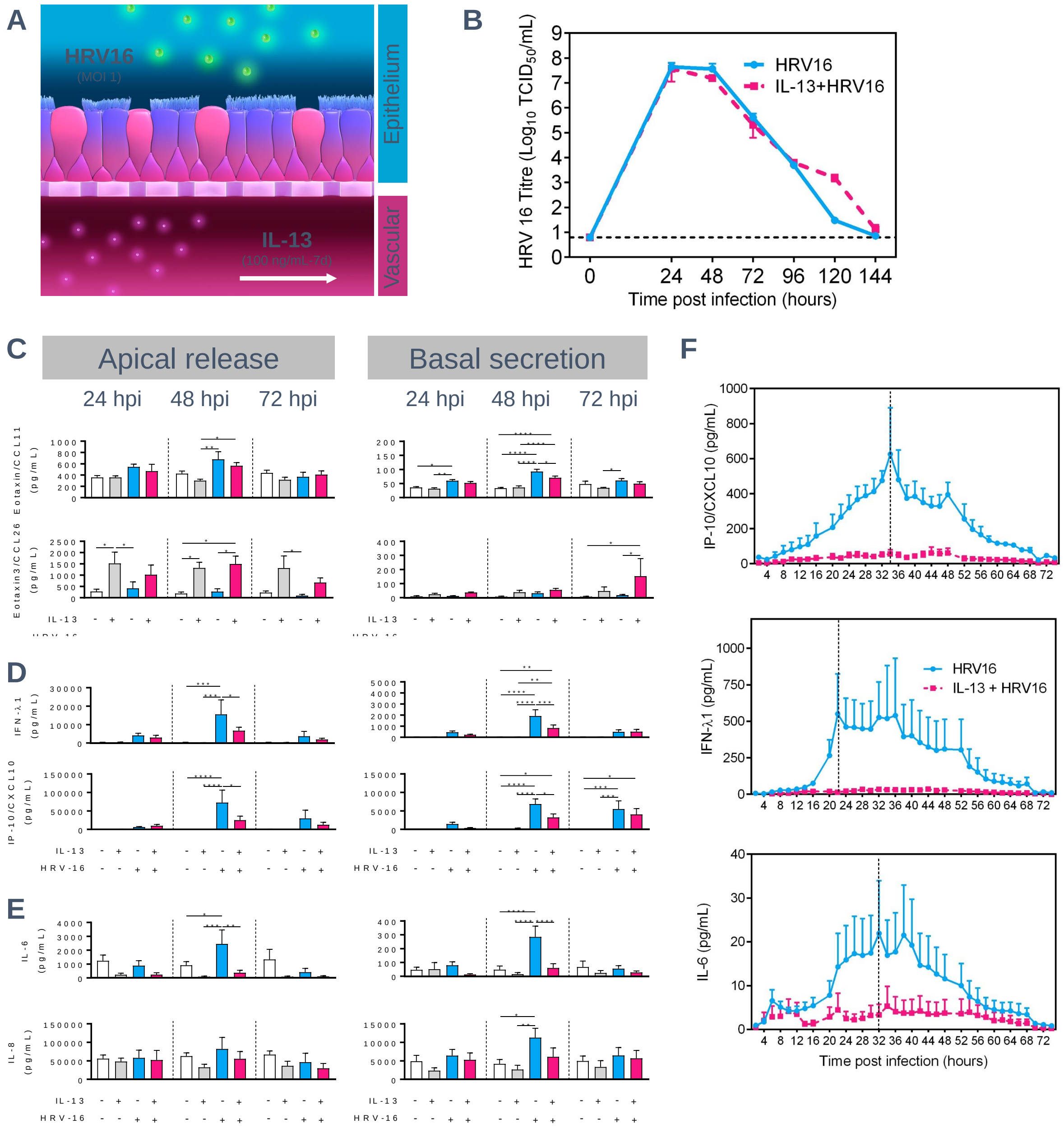

Figure 2. Modeling HRV-induced asthma exacerbation on chip and measuring inflammatory responses. (**A**) The severe asthma chip was generated by inducing features of Th2 asthma through vascular perfusion of IL-13 (100 ng/mL) and exacerbation through HRV16 epithelial infection (MOI 1). (**B**) Viral growth kinetic of HRV-16 following infection of the airway chip at an MOI~1 in the absence or presence of IL-13. HRV-16 was titrated in apical washes and data represent mean ± SEM log10 $TCID_{50}$/ml from 3 different donors with two to five biological replicates per donor. **(C-E)** The graphs show the effect of on polarized apical and basal release of CC chemokines (**C**), interferon and interferon-induced chemokines (**D**), and pro-inflammatory interleukins (E) by the combination of IL-13 treatment and HRV-16 infection in the exacerbated asthma chip at 24h, 48h and 72h post infection. (**F**) The graphs show a high resolution, kinetic profiles of insert IFN-λ1, IP-10/CXCL10and IL-6 response following HRV16 infection, with and without IL-13 treatment over 72 h. Data represent mean ±SEM of cells from three to four different donors, with one or two biological replicates (chips) per donor. Significance was determined by multiple comparison two-way ANOVA followed by Tukey's post-hoc correction; *P < 0.05, **P < 0.01, ***P < 0.001, ****P < 0.0001.

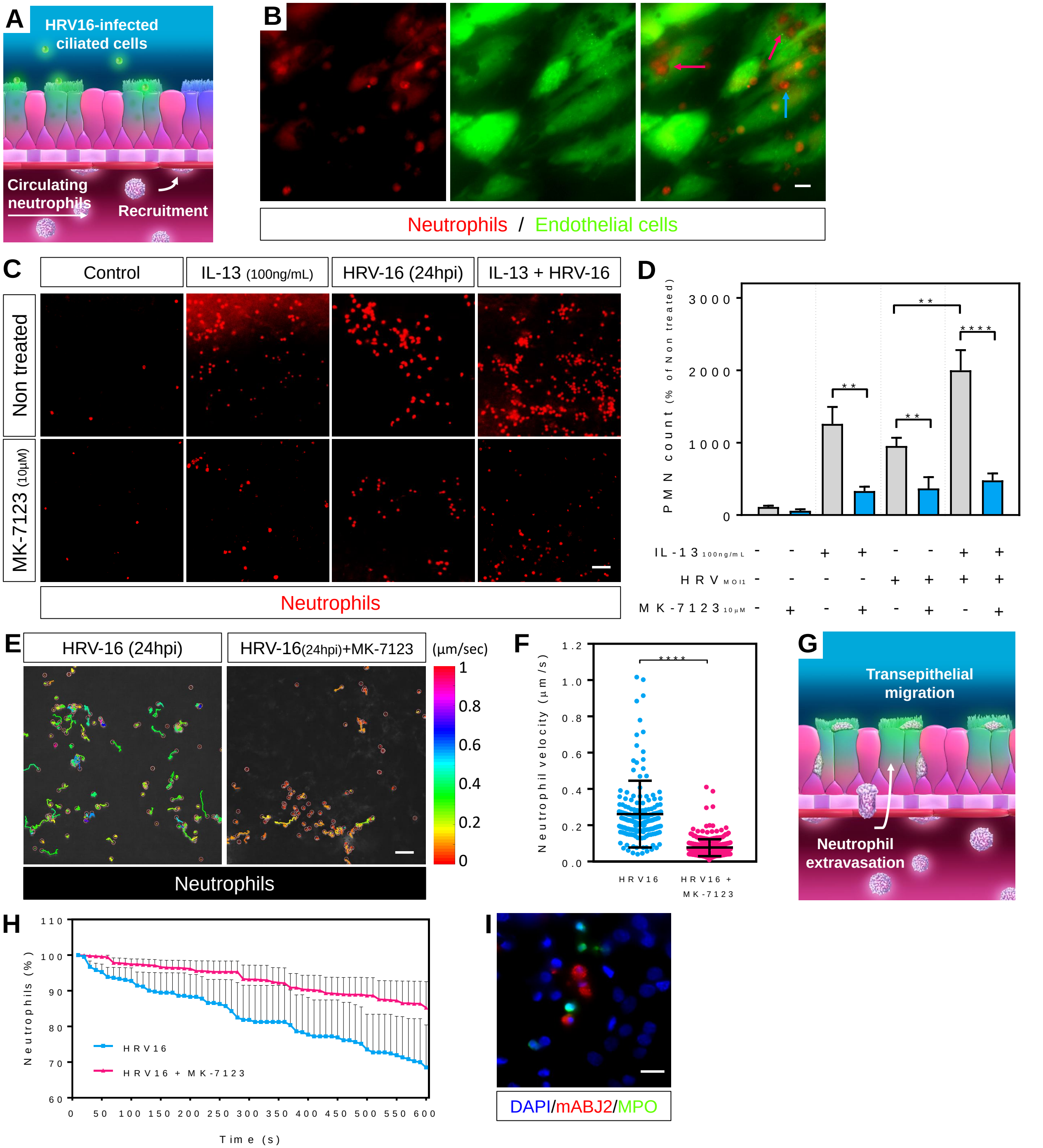

Fig 3. Assessing and modulating IL-13- and HRV-induced neutrophil recruitment and infiltration on chip. (**A**) Schematic diagram of the severe asthma chip depicting the neutrophil recruitment assay. (**B**) Micrographs showing paracellular and transcellular transmigration of neutrophil live-stained (red) through GFP-expressing endothelial cells (green). Obvious transcellular diapedesis events are indicated by the pink arrows while the blue arrow points at a paracellular migration. Scale bar, 10 µm. (**C**) Fluorescence microscopic imaging of chips perfused through the microvascular channel under physiological conditions (shear stress, 1 dyn/cm^2) for 5 min with freshly isolated CellTracker red−labeled human neutrophils showing recruitment to the endothelium stimulated or not with a combination of IL-13, HRV-16 and a CXCR2 antagonist (MK-7123 - 10µM). Scale bar, 50 µm. (**D**) Quantification of neutrophil recruitment from (**C**). (**E**) Schematic diagram of neutrophil diapedesis taking place in the severe asthma chip. (**F**) Fluorescence imaging tracking neutrophil velocity at the endothelial surface in HRV-16 infected chips, in absence (left) or presence (right) of the CXCR2 antagonist. Scale shows color coded velocity values in µm/sec; Scale bar, 50 µm. (**G**) Quantification of neutrophil velocity in HRV16 infected chips with or without MK-7123 (10µM). (**H**) The graph shows the disappearance of neutrophils (expressed in % of starting count) due to transmigration from the vascular wall to the epithelial lumen in HRV16 infected chips in absence or presence of MK-7123 (10µM). (**I**) Immunofluorescence micrograph of an HRV16 infected chip showing human neutrophil stained for myeloperoxidase (green) that have migrated to the epithelial lumen among HRV16 infected epithelial cells (red). Scale bar, 20 µm. Data represent mean ± SEM from three different donors with two biological replicates (chips) per donor.

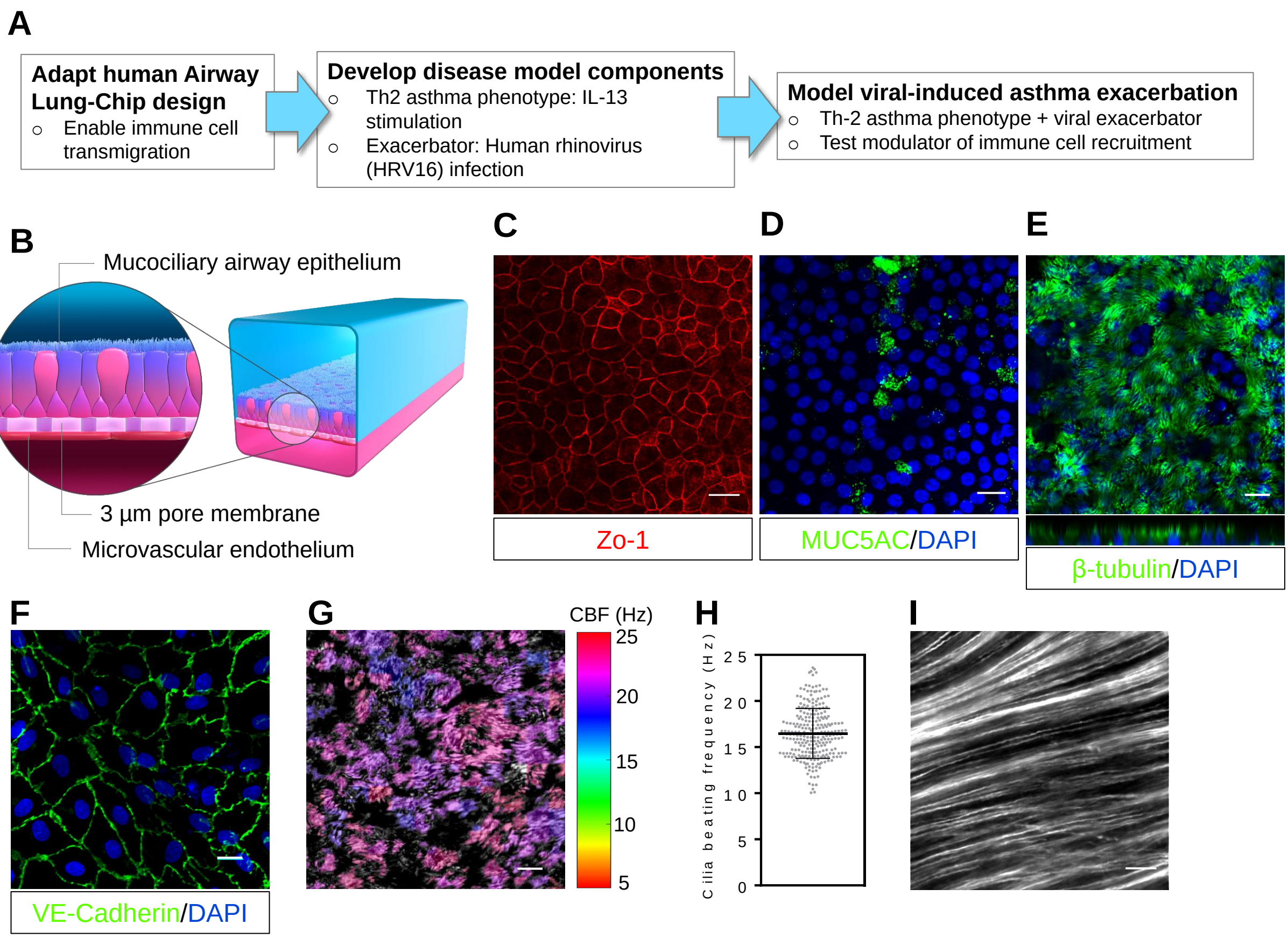

Supplementary figure 1. The human Airway chip. **A**) Overview of approach taken in this study to model asthma exacerbation and demonstrate feasibility of compound testing. (**B**) Functionally augmented Airway Lung-Chip design has 3-µm pore membrane for enabling neutrophil transmigration between the endothelial and epithelial channel. (**C**) The differentiated airway epithelium on the top channel exhibits continuous tight junctional connections on-chip, as demonstrated by Zo-1 staining (red). Scale bar, 20 µm. (**D-E**) The well-differentiated human airway epithelium generated on-chip also contains goblet cells stained for MUC5AC (green) and demonstrates extensive coverage of ciliated cells labelled for β-tubulin (green). Scale bar, 20 µm. (**F**) The human (lung blood microvascular) endothelial monolayer formed in the bottom channel of the chip features continuous adherens junctions between adjacent cells, as indicated by VE-Cadherin staining (green). Scale bar, 10 µm. All images are representative of two to five independent experiments performed with cells from three different donors. (**G**) Graphic representation of cilia beating frequency (CBF) on-chip generated from a high speed recording of cilia beating in a representative field of view. Scale shows color coded CBF values in Hz. Scale bar, 20 µm. (**H**) The graph shows the cilia beating frequency measured in 5-10 random on-chip fields of view and each dot represents regions of ciliary beating. Data have been recorded in cells from three different donors and are presented as mean ± SD. (**I**) Time lapse composite image of a 5 sec recording of 1-µm fluorescent microbeads suspended in PBS and introduced in the top channel. The path lines reveal the mucociliary transport of the differentiated hAECs. Scale bar, 20 µm.

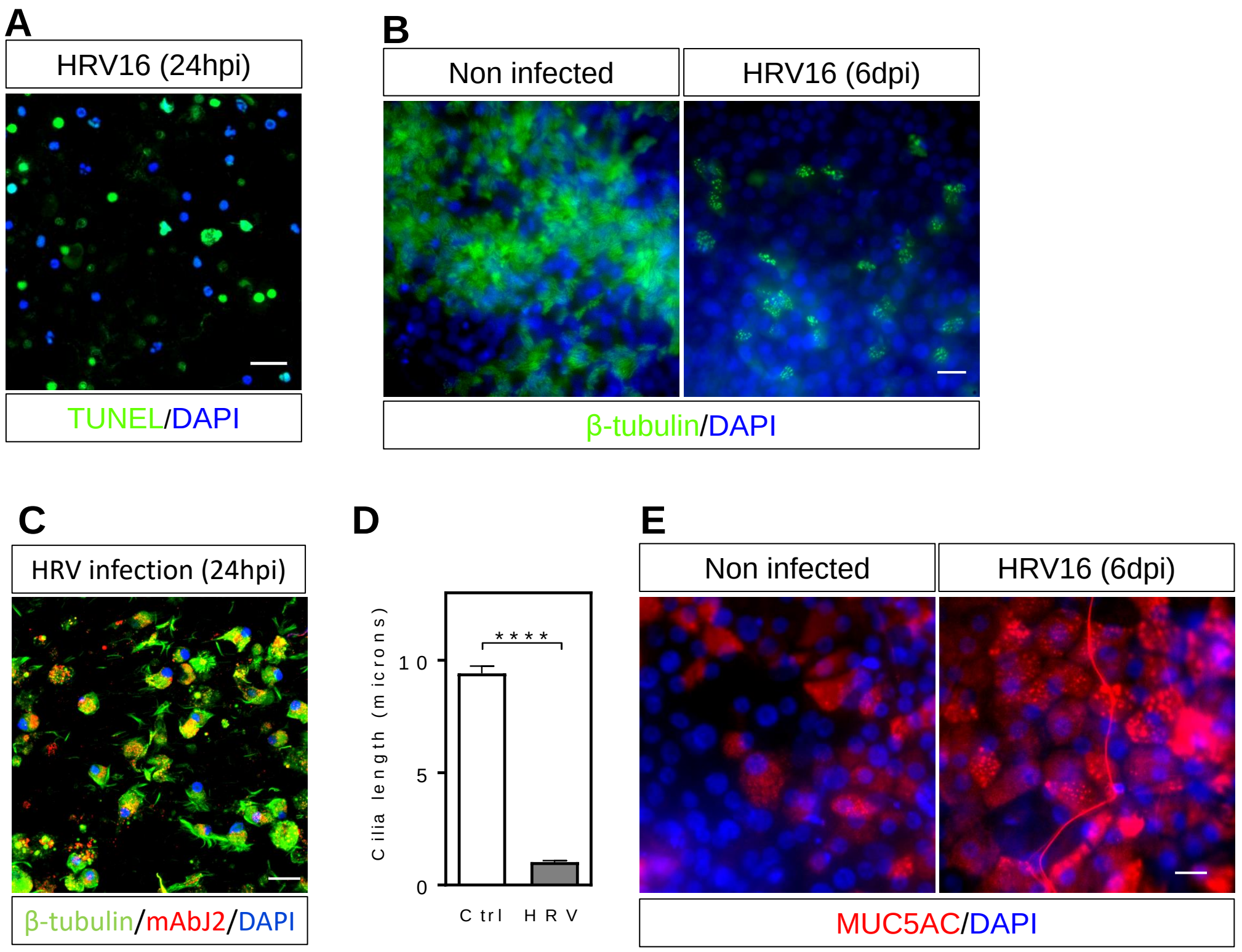

Supplementary figure 2. HRV infection causes cytopathic effects and epithelial remodeling. (**A**) Fluorescence confocal micrograph of detached epithelial cells stained using the TUNEL assay showing nuclei of apoptotic (green) and non apoptotic (blue) cells. Scale bar, 20 µm. (**B**) Immunofluorescence images of the differentiated epithelium non infected (left) or fixed at 6 days post HRV16 infection (right) and stained for β-tubulin (green) and DAPI (blue). Scale bar, 20 µm. (**D**) Confocal image of the cells collected in an apical wash 24 h following HRV16 infection of an airway chip showing the extend of ciliated cells destruction. Note the presence of individual cilia (green) in the apical wash. Scale bar, 20 µm. (**D**) Quantification of the length of cilia on multiciliated cells 6 d post HRV16 infection. Data represent mean ± SEM; Significance was determined by unpaired Student's t-test; ****$P < 0.0001$. (**E**) Immunofluorescence images of the differentiated epithelium non infected (left) or 6 days post HRV16 infection (right) and stained for MUC5AC (red) and DAPI (blue). Scale bar, 20 µm.

FIGURE 3

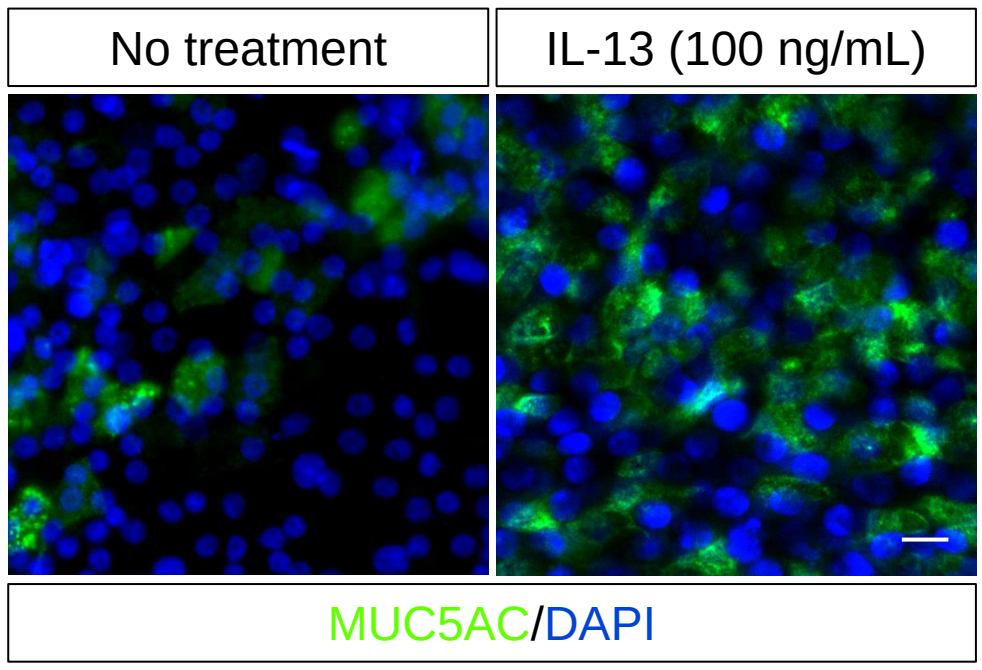

Supplementary Figure 3 . IL-13 induces goblet cell hyperplasia. Immunofluorescence confocal views of differentiated airway epithelium cultured at air-liquid interface for 3 weeks on-chip in the absence (left) or presence (right) of IL-13 (100 ng/mL) for 7 days showing epithelium stained for the goblet cell marker MUC5AC (green) and nuclei (blue). Scale bar, 20 µm (applies to both views); images are representative of two independent experiments performed on cells from three different donors.

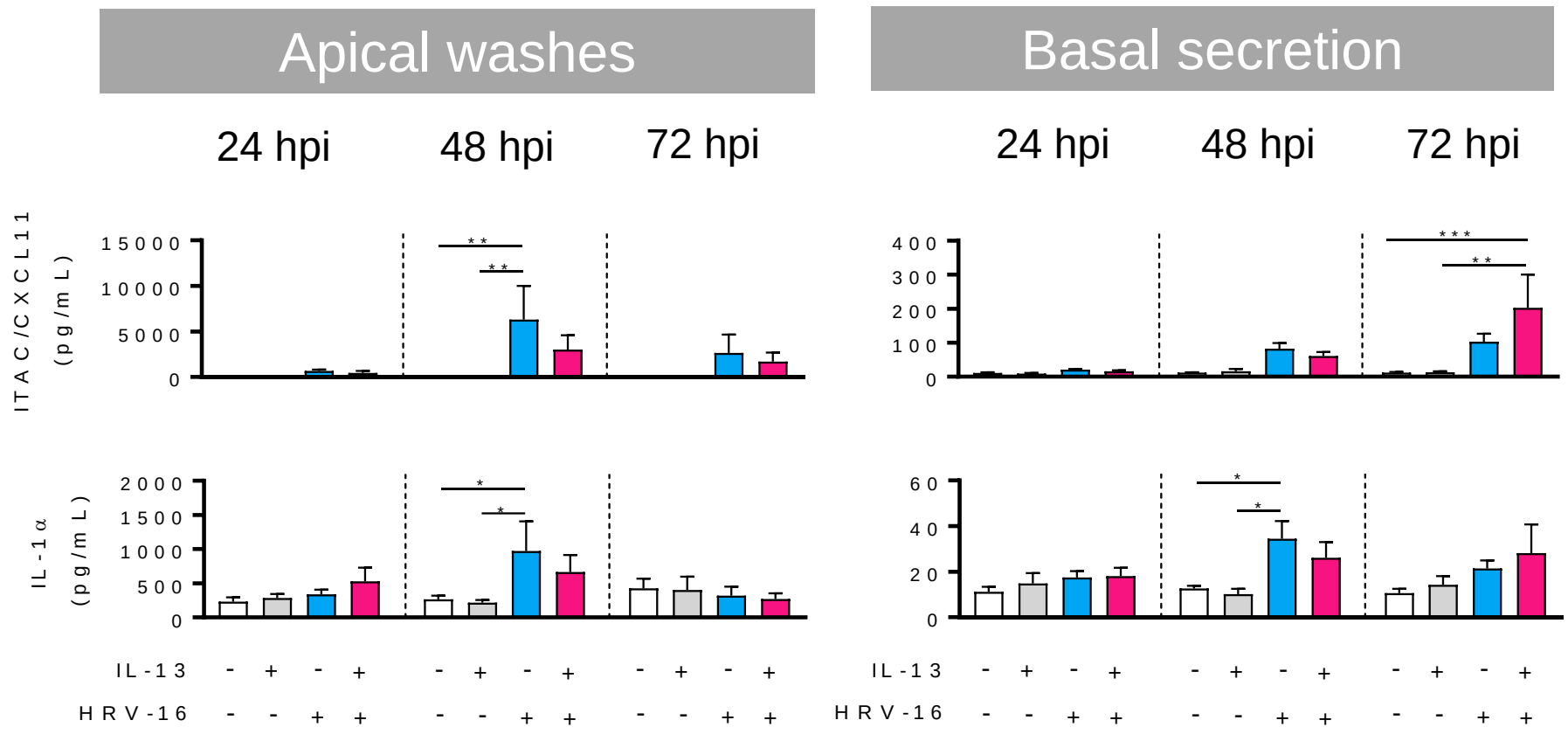

Supplementary figure 4. The graphs show the effect on polarized apical and basal release of CXCL11 and IL-1α by the combination of IL-13 treatment and HRV-16 infection in the severe asthma-on-a-chip at 24h, 48h and 72h post infection. Data represent mean ±SEM of cells from three to four different donors, with one or two biological replicates (chips) per donor. Significance was determined by multiple comparison two-way ANOVA followed by Tukey's post-hoc correction; *P < 0.05, **P < 0.01, ***P < 0.001.

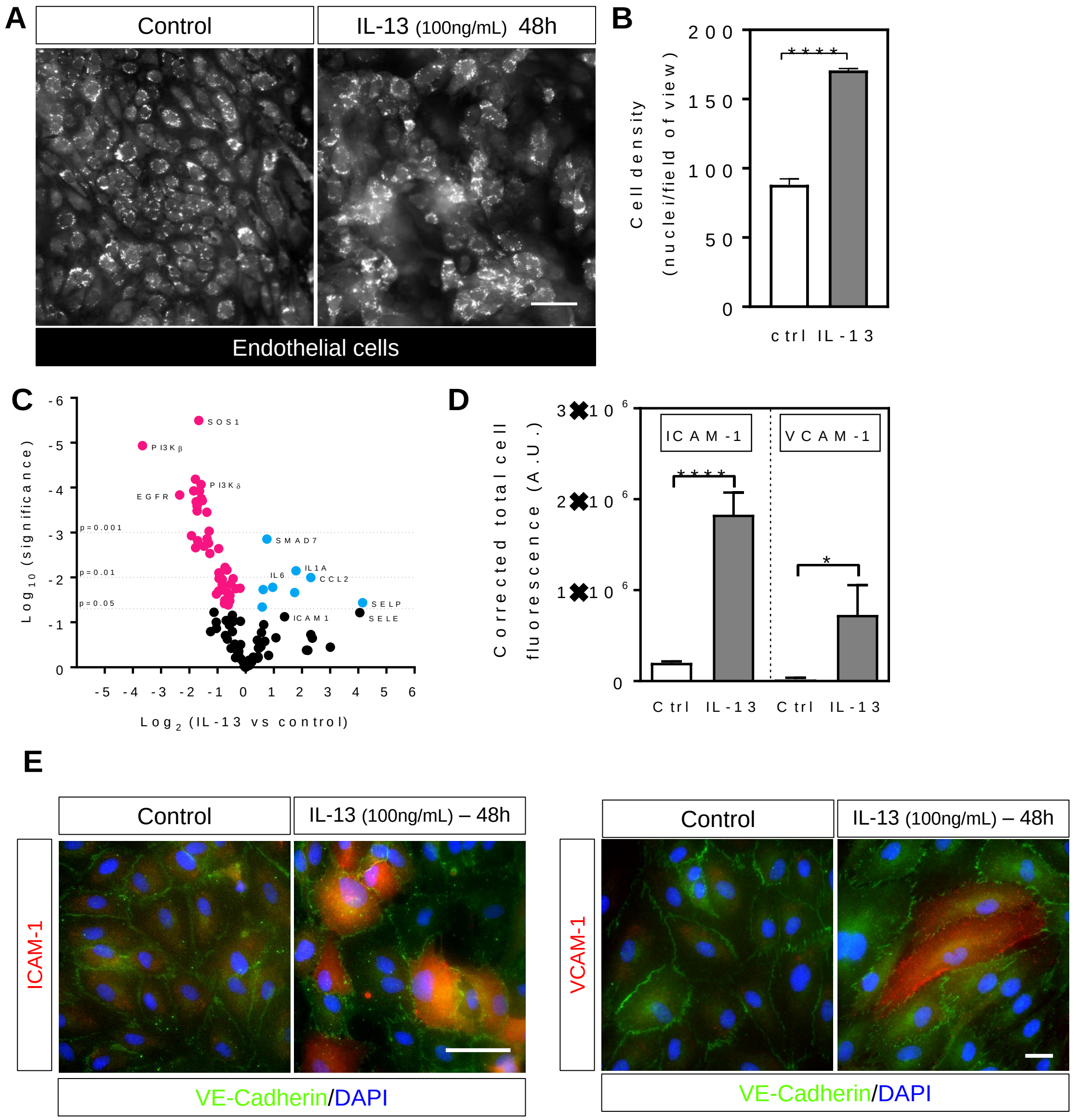

Supplementary figure 5. IL-13 induces aggregation and activation of endothelial cells. (**A**) Fluorescence micrographs of GFP-expressing endothelial cells co-cultured with well differentiated airway epithelial cells on chip, in absence (left) or presence (right) of IL-13 (100ng/mL) for 48h. Scale bar, 50 µm. (**B**) Quantification of endothelial cell density in absence or presence of IL-13 (100 ng/mL) for 48h. (**C**) Volcano plot showing gene expression of IL-13 (100ng/mL) treated endothelial cells compared to untreated group. Data were analyzed using a two-stage step-up method of Benjamini, Krieger and Yekutieli. (**D**) Effect of IL-13 (100ng/mL) on endothelial cell adhesion molecules ICAM-1 and VCAM-1 expression, as measured using fluorescence measurement. Data represent mean ±SEM of n=3 replicates. Significance was determined by unpaired Student's t-test; *P < 0.05, ****P < 0.0001. (**E**) Fluorescent micrograph of human pulmonary microvascular endothelial cells in presence and absence of IL-13 (100 ng/mL) for 48h and stained for adhesion molecules ICAM-1 and VCAM-1 (red), and VE-Cadherin (green). Nuclei were counter stained with DAPI (blue). Scale bar, 20 µm.

Donor #	AGE	SEX	SMOKING
1	5 yo	F	N
2	21 yo	M	N
3	18 yo	M	Y
4	18 yo	F	N

Supplementary table 1. Age and sex of donors used in this study.

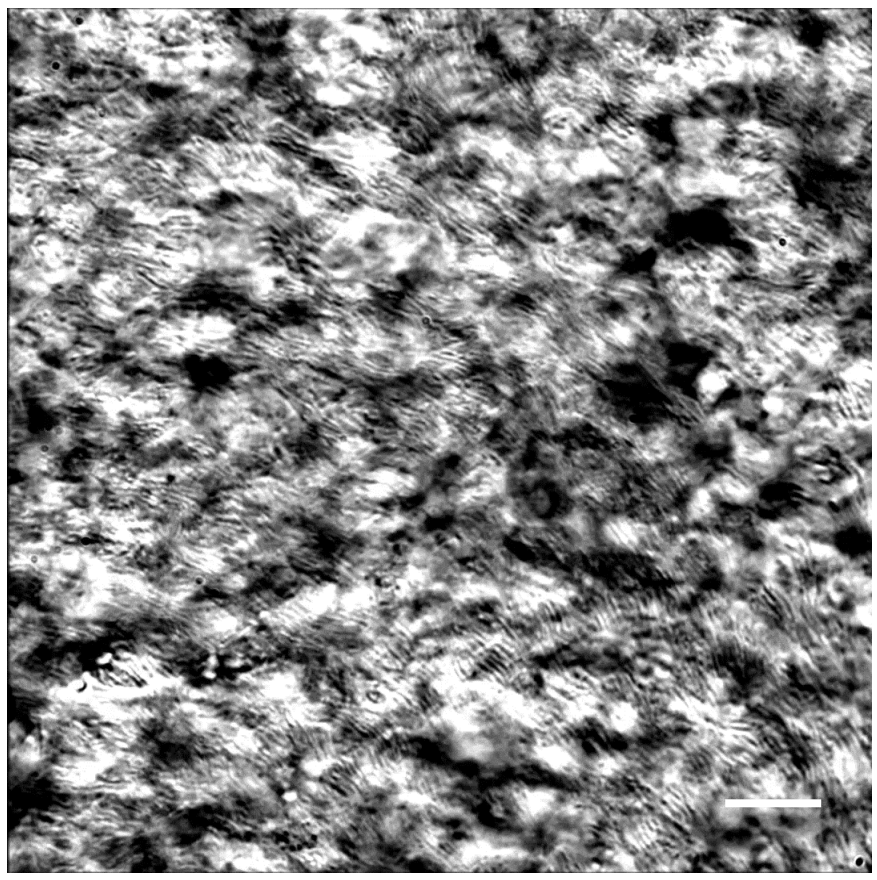

Supplementary movie 1. Real time phase contrast microscopic imaging of well differentiated human airway epithelial cells cultured inside the airway chip for 21 days on a 3 um pore membrane showing extensive coverage of synchronized cilia beating. Scale bar, 20 µm.

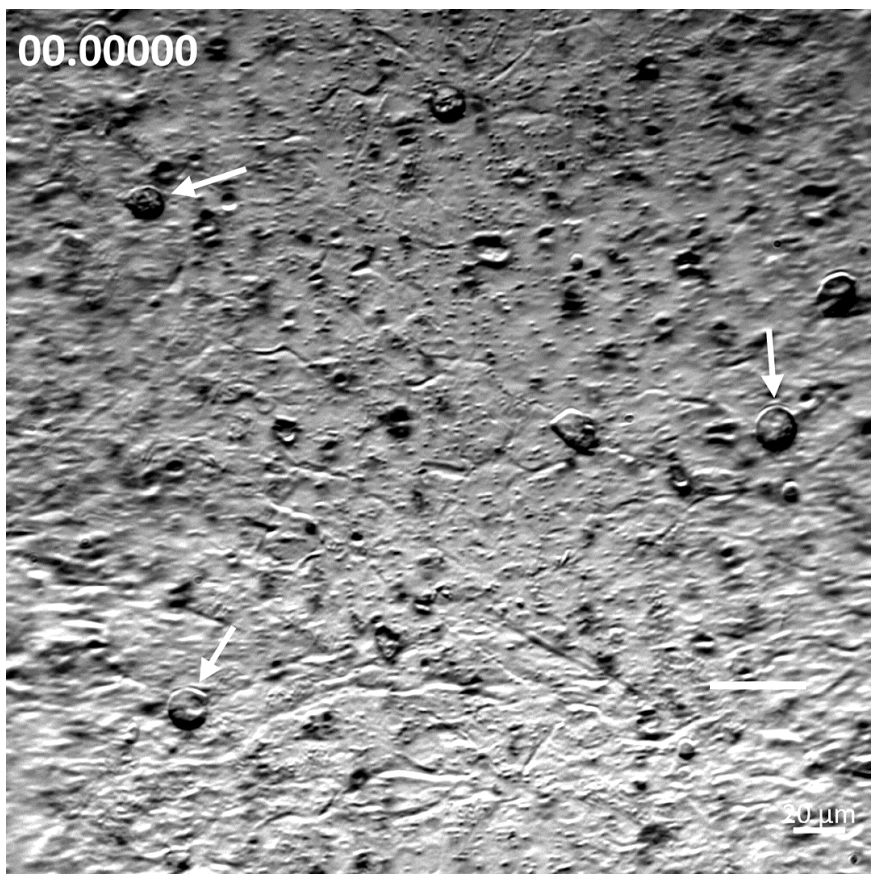

Supplementary movie 2. Real time phase contrast microscopic imaging of HRV16-infected airway chips (24hpi) showing rounded ciliated detaching from the epithelium (white arrows). Scale bar, 20 µm.

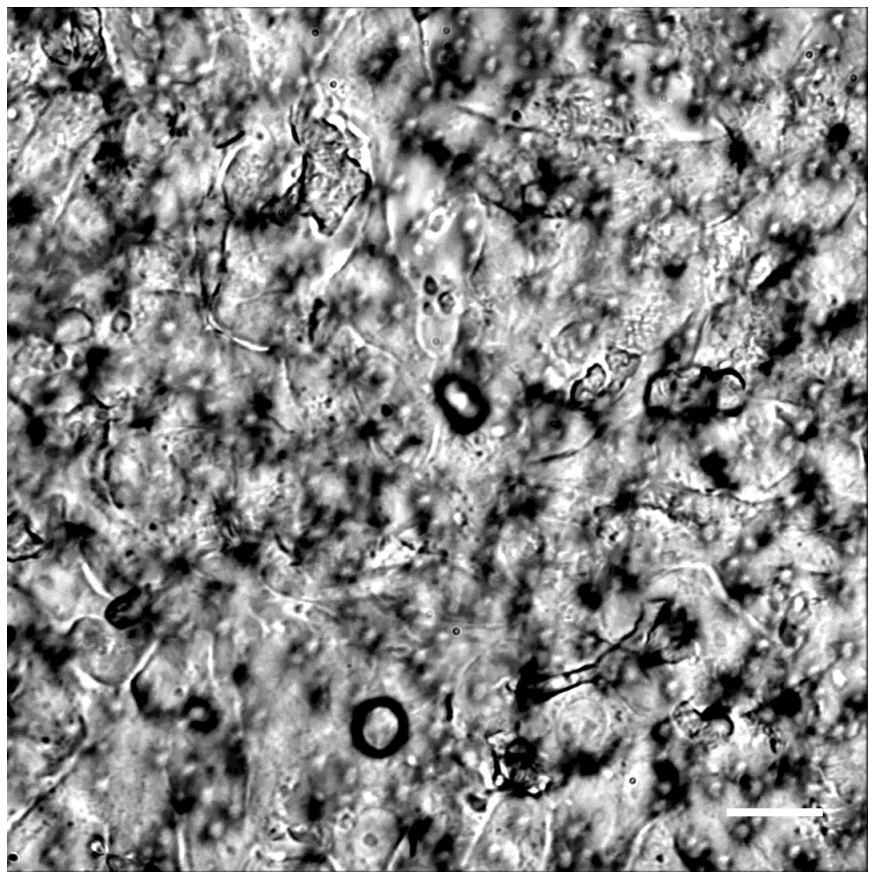

Supplementary movie 3. A movie showing phase contrast microscopic imaging of well differentiated human airway epithelial cells cultured inside the airway chip for 21 days on a 3 µm pore membrane and infected with HRV16 for 72 h. Scale bar, 20 µm.

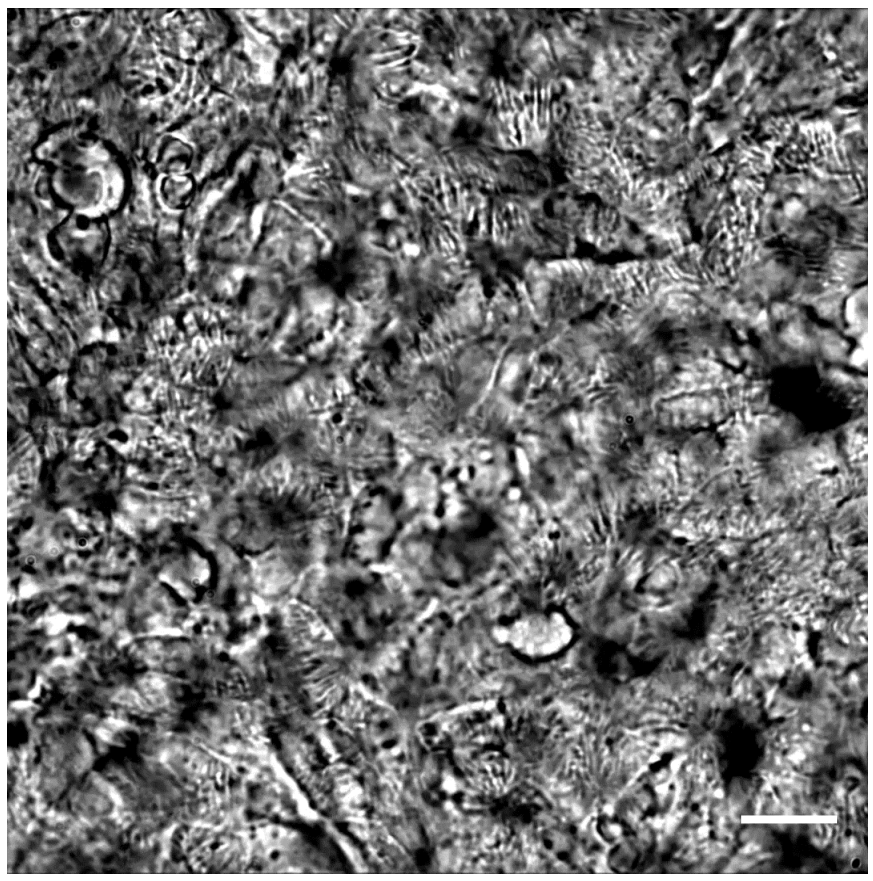

Supplementary movie 4. A movie showing phase contrast microscopic imaging of well differentiated human airway epithelial cells cultured inside the airway chip for 21 days on a 3 µm pore membrane and treated with IL-13 (100 ng/mL) for 7 d. Scale bar, 20 µm.

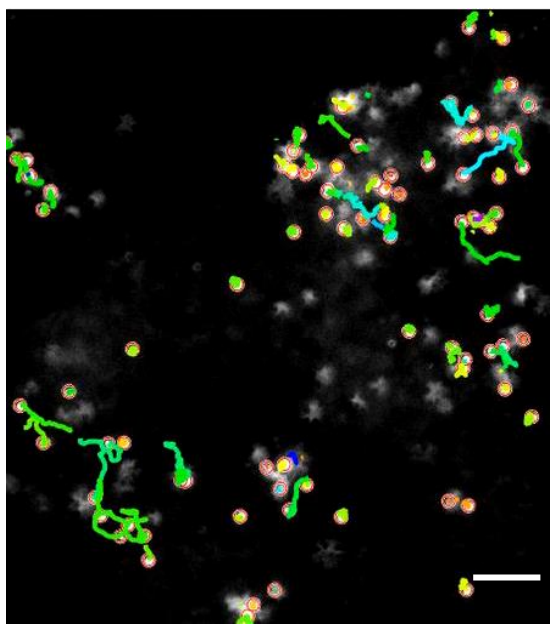

Supplementary movie 5. A movie showing movement tracking of fluorescently labelled human neutrophils recruited to the surface of the microvascular endothelium 24 post HRV16 infection on chip. Scale bar, 50 µm.

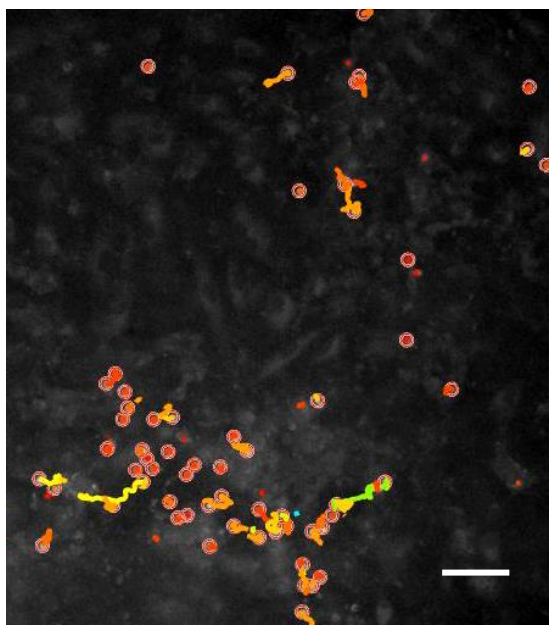

Supplementary movie 6. A movie showing movement tracking of fluorescently labelled human neutrophils recruited to the surface of the microvascular endothelium 24 post HRV16 infection and treated with the CXCR2 inhibitor, MK-7123 (10µM) on chip. Scale bar, 50 µm.

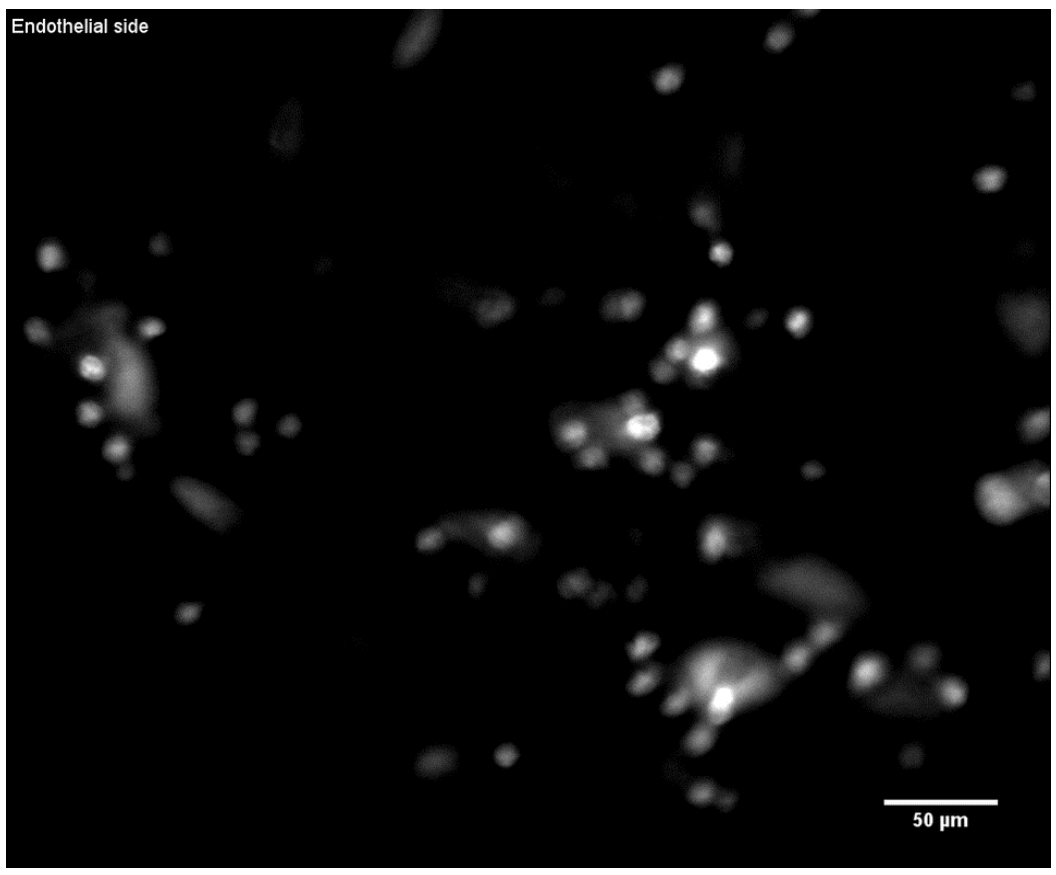

Supplementary movie 7. A movie of an orthogonal sectioning of a chip from the vascular to the epithelial compartment showing labelled neutrophil (white) at the surface of the microvascular endothelium and neutrophil that have crossed the membrane and transmigrated towards the epithelium. Scale bar, 50 µm.